iScience, Volume *24*

Supplemental information

Synergetic surface charge transfer doping and passivation toward high efficient and stable perovskite solar cells

Xing Guo, Jie Su, Zhenhua Lin, Xinhao Wang, Qingrui Wang, Zebing Zeng, Jingjing Chang, and Yue Hao

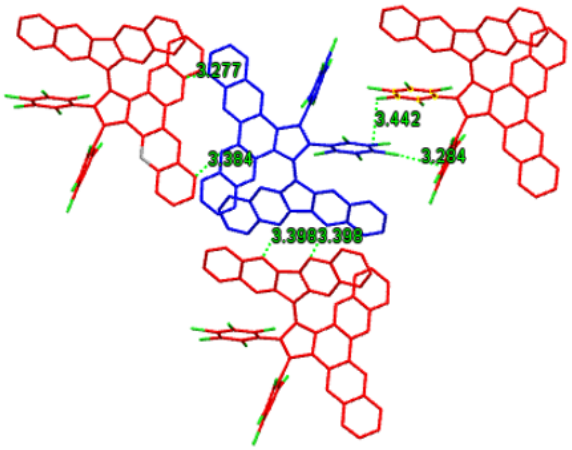

Figure S1. The crystal packing of FDC-2-5Cl, and green represents chlorine. The typical intermolecular distance and molecular interactions between different part. Related to Figure 1.

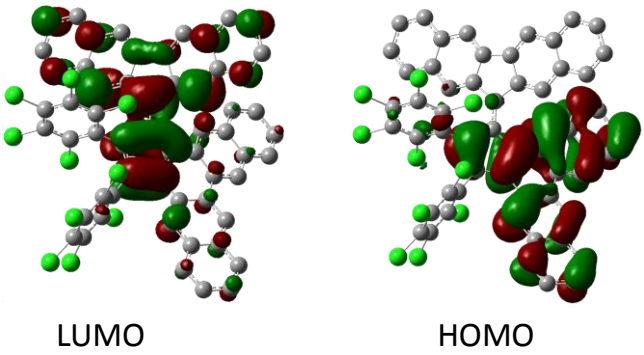

Figure S2. Calculated molecular orbital profiles of the HOMO and LUMO of FDC-2-5Cl. Related to Figure 1.

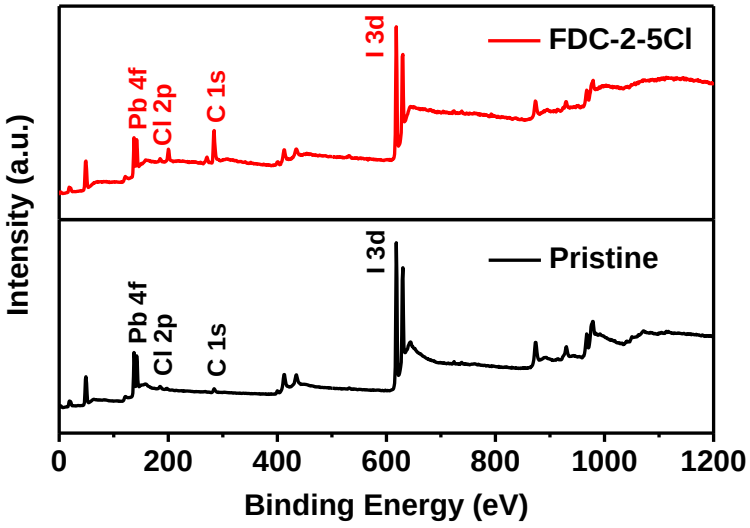

Figure S3. The full XPS spectra of perovskite films without and with FDC-2-5Cl treatment. Related to Figure 1.

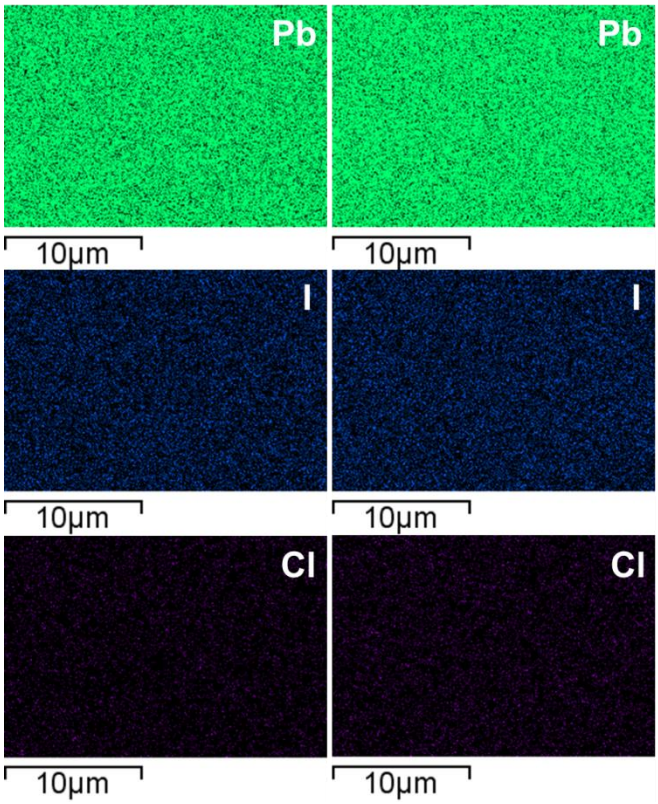

Figure S4. The SEM-EDS mapping images of perovskite films without (left) and with (right) FDC-2-5Cl treatment. Related to Figure 1.

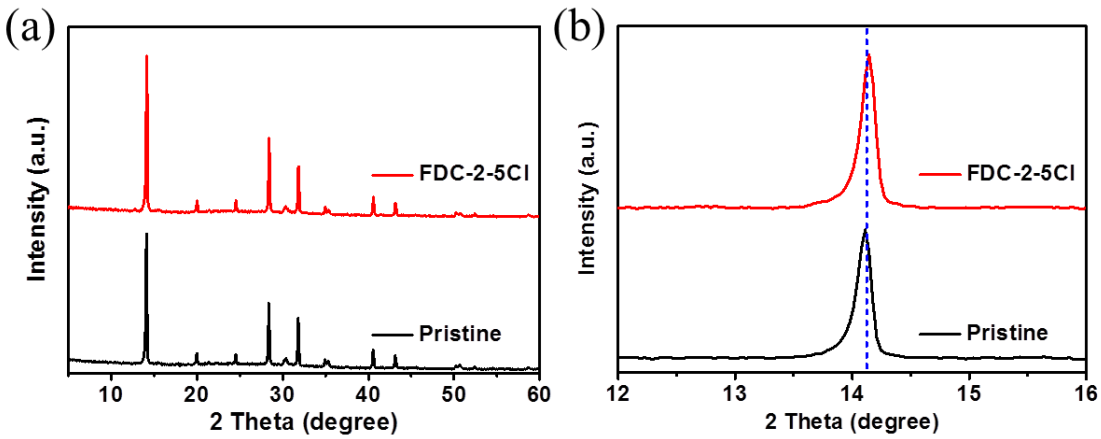

Figure S5. (a) XRD patterns of perovskite films without and with FDC-2-5Cl treatment. (b) Zoom-in image of (110) peak of Figure a. Related to Figure 1.

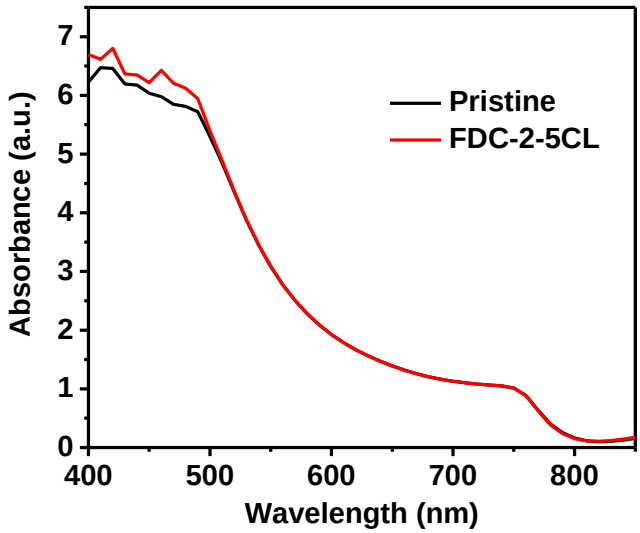

Figure S6. UV-vis absorption spectra of perovskite films without and with FDC-2-5Cl treatment. Related to Figure 2.

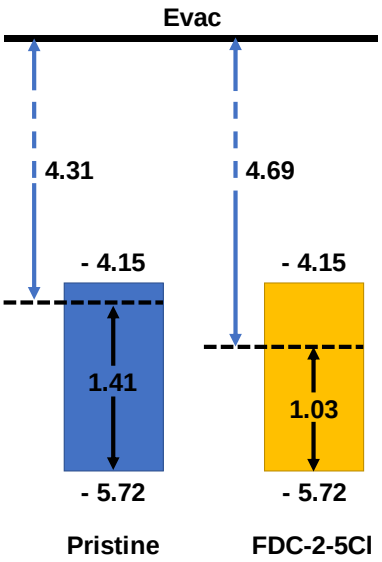

Figure S7. Energy level schemes of perovskite film without and with FDC-2-5Cl treatment derived from UPS spectra. Related to Figure 2.

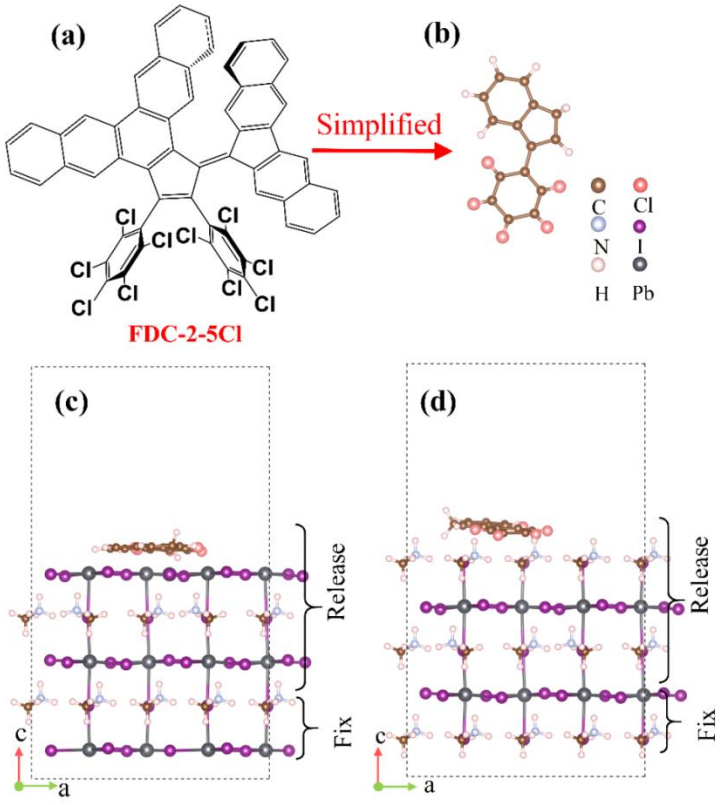

Figure S8. Side views of (a) FDC-2-5Cl and (b) simplified FDC-2-5Cl. (c) Simplified FDC-2-5Cl treated $MAPbI_3$ (001) surface with with V_I and (d) simplified FDC-2-5Cl treated $MAPbI_3$ (001) with I_{Pb}. Related to Figure 3.

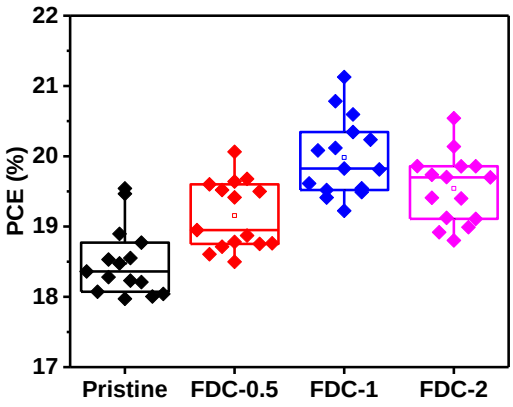

Figure S9. PCE distribution of PSCs with different concentrations FDC-2-5Cl treatment, 0.5 mg/mL (FDC-0.5), 1 mg/mL (FDC-1), and 2 mg/mL (FDC-2). Related to Figure 4.

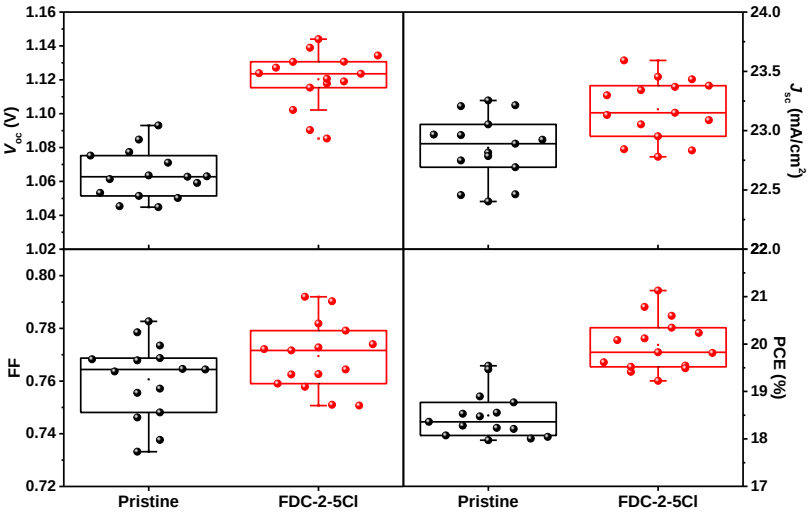

Figure S10. Device performance distribution of PSCs without and with FDC-2-5Cl treatment. Related to Figure 4.

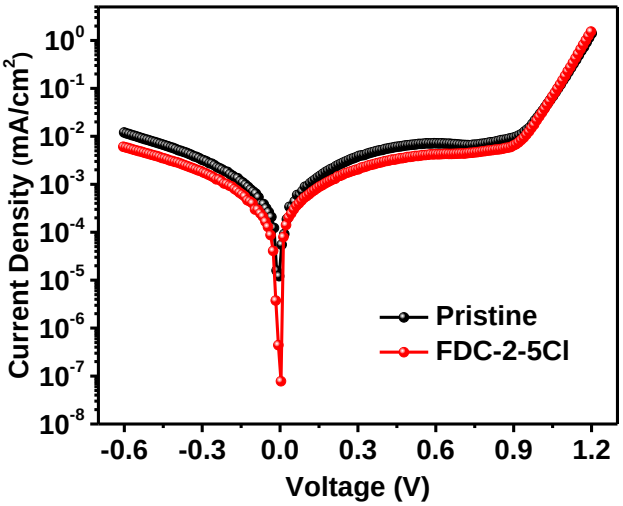

Figure S11. The dark *J* - *V* characteristics of PSCs without and with FDC-2-5Cl treatment. Related to Figure 4.

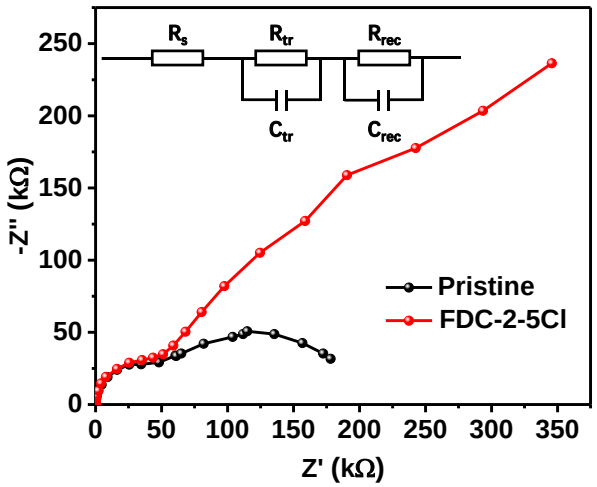

Figure S12. EIS spectra of PSCs without and with FDC-2-5Cl treatment. Related to Figure 4.

Table S1. The electrical characters of FDC-2-5Cl. Related to Figure 1.

Compound	HOMO (eV)	LUMO (eV)	μ_e $cm^2V^{-1}s^{-1}$	μ_h $cm^2V^{-1}s^{-1}$
FDC-2-5Cl	-5.45	-3.91	2.57×10^{-4}	1.06×10^{-4}

Table S2. Fitting parameters of TRPL curves. Related to Figure 4.

Samples	τ_1 (ns)	A_1	τ_2 (ns)	A_2	τ_{ave} (ns)
Perovskite	24.60	0.28	101.25	0.72	94.60
Perovskite (FDC-2-5Cl)	15.11	0.46	82.76	0.54	73.52
Perovskite/Spiro-OMeTAD	4.00	0.99	88.63	0.01	23.53
Perovskite (FDC-2-5Cl)/Spiro-OMeTAD	3.61	0.99	62.08	0.01	9.92

Table S3. Fitting parameters of EIS spectra. Related to Figure S12.

Samples	R_s (Ω)	R_{tr} (Ω)	C_{tr} (F)	R_{rec} (Ω)	C_{rec} (F)
Pristine	25.44	5.64×10^{4}	6.80×10^{-9}	1.08×10^{5}	1.25×10^{-7}
FDC-2-5Cl	22.50	2.70×10^{4}	6.87×10^{-9}	3.20×10^{6}	1.70×10^{-7}

Table S4. The comparison of device characteristics passivated by the organic molecule in our work and related literatures. Related to Figure 4.

Passivation molecule	PCE	V_{oc}	Hysteresis index	Long-term stability	References
FDC-2-5Cl	21.16 %	1.14 V	2.45 %	88 %, 1008h, in air, 60% RH, 20-30 ^{o}C	This work
$TBAPF_6$	21.23 %	1.103 V	0.4 %	90 %, 400 h, in air, 45% RH, room temperature	(Xiong et al., 2021)
ML	21.4 %	1.16 V	3.74 %	70.6 %, 96 h, 70% RH	(Wu et al., 2020)
F5PEA	21.10 %	1.196 V	0.57 %	83 %, 720 h, 45-60% RH	(Ye et al., 2020)

TCPBr	20.13 %	1.14 V	5.4 %	90.7 %, 1000 h, 60-80 %RH, room temperature	(He et al., 2020)
TPFP	21.04 %	1.16 V		63 %, 336 h, 75% RH	(Yang et al., 2020)
TBPO	22.1 %	1.14 V	5.88 %	90%, 3500 h, in dark and ambient condition	(Li et al., 2020)

Transparent Methods

Materials: All materials Tin (IV) oxide (SnO_2, 15 % in H_2O colloidal dispersion, Alfa Aesar), lead iodide (II) (PbI_2, 99.999 %, Alfa), lead (II) chloride ($PbCl_2$, 99.999 %, Alfa), cesium iodide (CsI, 99.998 %, Alfa), Methylammonium iodide (MAI, 99.8 %, Dyesol), Formamidinium iodide (FAI, 99.8 %, Dyesol) and spiro-OMeTAD (Xi'an Polymer Light Technology Corp.) are purchased without further purification. All solvent, N,N-Di-methylformamide (DMF, 99.8 %), isopropanol (IPA, 99.5 %) and chlorobenzene (CB, 99.5 %) are purchased from Sigma-Aldrich.

Device Fabrication: The indium tin oxide (ITO) glass substrates (around 2×2.5 cm^2 in size, 10 Ω per square) were cleaned sequentially with detergent, deionized water, acetone, and ethanol in an ultrasonic wave for 20 min, respectively. The SnO_2 (15 % in H_2O colloidal dispersion) solution was diluted to 5 % and spin coated on the ITO substrates at 4000 rpm for 40 s and annealed at 150 °C for 30 min on a hot plate to form SnO_2 layer. After cooling down to room temperature, the substrates were transfered into a nitrogen-filled glove box. For the perovskite film fabrication, 1.36 M PbI_2, 0.24 M $PbCl_2$ and 0.08 M CsI were dissolved in the DMF and stirred for 3 h at 70 °C. 70 mg MAI and 30 mg FAI were dissolved in 1 mL IPA with 10 μL DMF added. After that, around 70 μL PbX_2 precursor solution was spin coated onto SnO_2 substrates at 3000 rpm for 45 s. Then, 200 μL MAI:FAI solution was spin coated onto the PbX_2 at 3000 rpm for 45 s. Then the samples were thermally annealed on a hot plate at 100 °C for 10 min. For the FDC-2-5Cl treatment, the FDC-2-5Cl was dissolved in CB at different concentration and spin-coated on the perovskite film and annealed 100 °C for 3 mins. The spiro-OMeTAD was spin-coated on the top of the perovskite layer at 4000 rpm for 45 s. The spiro-OMeTAD solution was prepared by dissolved 72.5 mg spiro-OMeTAD in 1 mL chlorobenzene and added 17.5 μL Li-TFSI solution (520 mg/mL in acetonitrile), 28.8 μL FK209 solution (300 mg/mL in acetonitrile) and 28.8 μL 4-tertbutylpyridine (tBP). Finally, 100 nm Ag was thermally evaporated on the top of spiro-OMeTAD as the electrodes. The area of the device was 7.5 mm^2 defined by the metal mask. For the electron-only device (glass/ITO/SnO_2/perovskite(FDC-2-5Cl)/PCBM/Ag) and hole-only device (glass/ITO/NiO/perovskite(FDC-2-5Cl)/spiro-OMeTAD/Ag), the fabrication methods of SnO_2, perovskite, FDC-2-5Cl, spiro-OMeTAD and Ag are same with the method used in PSCs fabrication. The NiO layer was fabricated by a combustion method. The NiO precursor was prepared by dissolving 270.79 mg $Ni(NO_3)_2 \cdot 6H_2O$ in 2-methoxyethanol (10 mL). After the solution was stirred at 50 °C for 1 h, 100 μL

acetylacetone was added to the solution, and then the solution was further stirred overnight at room temperature. The NiO layer was fabricated by spin-coating the precursor solution on ITO substrates at 3000 rpm for 45 s and annealed at 250 °C for 45 min. The PCBM layer was fabricated by spin-coating the PCBM solution (20 mg/mL in chlorobenzene) on the top of the perovskite layer at 2000 rpm for 40 s. ***Characterization:*** The current density - voltage (*J* - *V*) characteristics of PSCs were measured under AM 1.5 G irradiation (100 mW cm^{-2}) by using a Keithley 2400 source meter, and the solar simulator (XES-70S1) was calibrated against an NREL certified silicon reference solar cell. The IPCE was measured by a solar cell quantum efficiency measuring system (SCS10-X150, Zolix instruments. Co. Ltd.). All the tests were carried out in ambient air in a temperature of 28 - 35 °C and a relative humidity of approximately 30 - 80 %. The *C* - *V* and EIS were measured by an electrochemical workstation (DH7001). The morphology of the perovskite layer was measured by SEM (JSM-7800F). XRD test was conducted on Bruker D8 Advance XRD. PL and TR-PL were measured using the Pico Quant Fluotime 300 by using a 510 nm picosecond pulsed laser. The UV-vis absorption spectra were recorded using an ultraviolet-visible spectrophotometer (Perkin-Elmer Lambda 950). The water contact angle measurement was carried out by a contact angle meter (JC2000DM, Beijing Zhongyikexin Science and Technology Co. Ltd., Beijing, China). XPS measurements were performed by the Escalab 250Xi with a source of monochromatic Al-Ka (1486.6 eV). The UPS measurements were carried out using a He I (*hv* = 21.22 eV) source.

DFT calculation: All calculations were based on density functional theory (DFT)(Hohenberg and Kohn, 1964) as implemented in the Vienna ab initio simulation package (VASP)(Kresse and Furthmüller, 1996a, 1996b) code with projector augmented wave (PAW) method.(Blochl, 1994; Kohn and Sham, 1965; Kresse and Joubert, 1999) The Perdew-Burke-Ernzerhof (PBE) functional within the generalized gradient approximation (GGA) was employed to describe the exchange-correlation interaction.(Perdew et al., 1996) The van der Waals interaction is considered using DFT-D2 method. The plane-wave cut-off energy of 400 eV and Monkhorst-Pack k-point meshes spanning less than 0.02 $Å^{-3}$ in the Brillouin zone were chosen. All structures were relaxed until the residual force on each atom less than 0.01 eV/Å. The self-consistent convergence accuracy was set at 10^{-5} eV/atom in the structural calculation. The MAI and PbI terminated defective $MAPbI_3$ surfaces were modelled employing periodically repeated slabs using the (2 × 2) supercell with adsorbates on one side, as shown in Figure S8. The slabs were seven layers thick, and the bottom three layers were kept fixed in their bulk positions during relaxations. A vacuum region more than 15 Å in the z-direction in conjunction with the dipole correction to avoid the fictitious interaction with its periodic images. According to previous reports, the large FDC-2-5Cl molecular was separated into two parts to successfully obtain the effect of FDC-2-5Cl, as demonstrated in Figure S8.

Supplemental References

Blochl, P.E., 1994. Projector augmented-wave method. Phys. Rev. B 50, 17953–17979.

Hohenberg, P., Kohn, W., 1964. Inhomogeneous Electron Gas. Phys. Rev. 136, B864–B871.

Kohn, W., Sham, L.J., 1965. Self-Consistent Equations Including Exchange and Correlation Effects. Phys. Rev. 140, A1133–A1138.

Kresse, G., Furthmüller, J., 1996a. Efficiency of ab-initio total energy calculations for metals and semiconductors using a plane-wave basis set. Comput. Mater. Sci. 6, 15–50.

Kresse, G., Furthmüller, J., 1996b. Efficient iterative schemes for ab initio total-energy calculations using a plane-wave basis set. Phys. Rev. B 54, 11169–11186.

Kresse, G., Joubert, D., 1999. From ultrasoft pseudopotentials to the projector augmented-wave method. Phys. Rev. B 59, 1758–1775.

Perdew, J.P., Burke, K., Ernzerhof, M., 1996. Generalized Gradient Approximation Made Simple. Phys. Rev. Lett. 77, 3865–3868.

He, Q., Worku, M., Xu, L., Zhou, C., Lteif, S., Schlenoff, J.B., Ma, B., 2020. Surface passivation of perovskite thin films by phosphonium halides for efficient and stable solar cells. J. Mater. Chem. A 8, 2039–2046.

Li, H., Shi, J., Deng, J., Chen, Z., Li, Y., Zhao, W., Wu, J., Wu, H., Luo, Y., Li, D., Meng, Q., 2020. Intermolecular π–π Conjugation Self‐Assembly to Stabilize Surface Passivation of Highly Efficient Perovskite Solar Cells. Adv. Mater. 32, 1907396.

Wu, Z., Jiang, M., Liu, Z., Jamshaid, A., Ono, L.K., Qi, Y., 2020. Highly Efficient Perovskite Solar Cells Enabled by Multiple Ligand Passivation. Adv. Energy Mater. 10, 1903696.

Xiong, S., Dai, Y., Yang, J., Xiao, W., Li, D., Liu, X., Ding, L., Gao, P., Fahlman, M., Bao, Q., 2021. Surface charge-transfer doping for highly efficient perovskite solar cells. Nano Energy 79, 105505.

Yang, Z., Dou, J., Kou, S., Dang, J., Ji, Y., Yang, G., Wu, W.Q., Kuang, D. Bin, Wang, M., 2020. Multifunctional Phosphorus-Containing Lewis Acid and Base Passivation Enabling Efficient and Moisture-Stable Perovskite Solar Cells. Adv. Funct. Mater. 30, 1910710.

Ye, J.Y., Tong, J., Hu, J., Xiao, C., Lu, H., Dunfield, S.P., Kim, D.H., Chen, X., Larson, B.W., Hao, J., Wang, K., Zhao, Q., Chen, Z., Hu, H., You, W., Berry, J.J., Zhang, F., Zhu, K., 2020. Enhancing Charge Transport of 2D Perovskite Passivation Agent for Wide-Bandgap Perovskite Solar Cells Beyond 21%. Sol. RRL 4, 2000082.